

List of Responses

Responds to the Anonymous Referee #1's comments:

Special thanks for your good comments which are very useful for us to improve the paper.

1. Response to comment: Here are some questions on the additional numerical experiments shown in Fig. 3 (Box-plot of the PSO, WSA and ACPW methods for TC Fitow at 60 km resolution) of the revised manuscript. In Fig.2, we find large differences among the initial objective function values for the PSO, WSA and ACPW methods, and the one for the ACPW method is even approximately equal to the final objective function value obtained by the PSO method. Does this disparity exists in the numerical experiments shown in Fig. 3? If so, the comparison of the objective function values gained respectively by the PSO, WSA and ACPW methods cannot support the better optimization performance of the ACPW methods. Accordingly, the descending degree of the objective function value for the three methods should be compared.

Response: As Reviewer mentioned that the Fig. 2 is unsuitable in the revised manuscript. Actually, the purpose of using Fig. 2 is to illustrate the different performance of the PSO, WSA and ACPW methods, but we only use one group experiments. Hence, we delete it in the new revised manuscript.

And to answer the question “Does this disparity exists in the numerical experiments shown in Fig. 3?”, we did the statistical analysis of the first objective values, and plotted their distributions of the different methods in the new Fig. 3 in line 9-18, P. 8.

“ Since these three algorithms are all heuristic algorithms with randomness, and the initial inputs are generated by random way, the initial objective value is different for every running. To analyse the effect of initial objective values on the different algorithms, we exhibit the objective value scope of the PSO, WSA and ACPW algorithms after the first iteration in Fig. 3.

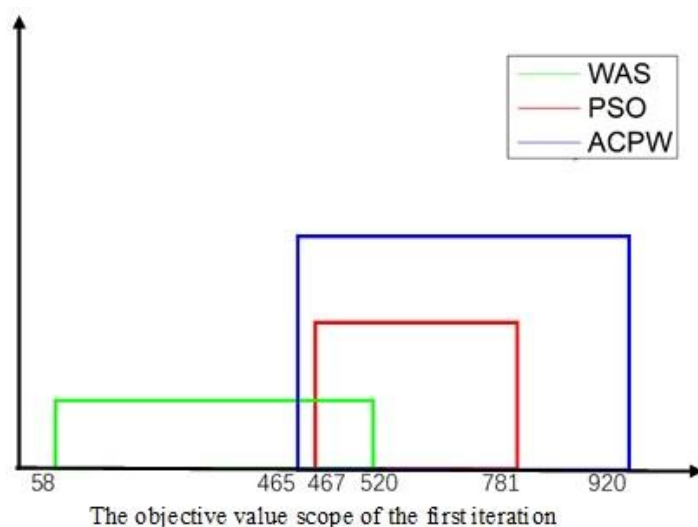


Figure 3: The first objective value scope of the PSO, WSA and ACPW methods. PSO is denoted as

the red line, the WSA is shown as the green line, and the ACPW algorithm is represented as the blue line.

In Fig. 3, for convenience, only integer is indicated in the coordinate system. In 10 experiments, the PSO has the narrowest scope from 467.1719 to 781.6482. The WSA and ACPW algorithms have similar value spans, which are wider than the PSO, but the objective values of the ACPW are higher. And the value scope is reasonable according to the characteristic of these three algorithms. The WSA has the strongest randomness, the PSO is the most stable, and the ACPW combines the advantages of the two. From the results, we cannot find the direct relationship between the initial objective value and the final result, but a better first objective value has a beneficial effect on finding the optimal value.”

As Reviewer suggested that we compared the changing degree of the objective function value for the three algorithms to illustrate the performance of the different algorithms, and the results were shown in the new Fig. 4 in line 19-29, P. 8.

“ To illustrate better performance of the ACPW algorithm, we calculate the average objective value of every step of 10 program results, and then obtain the change degree between the two iterations. We draw them in Fig. 4. If the objective value is continuously changing, then the algorithm has better global searching ability; otherwise the algorithm tends to fall in local optimization.

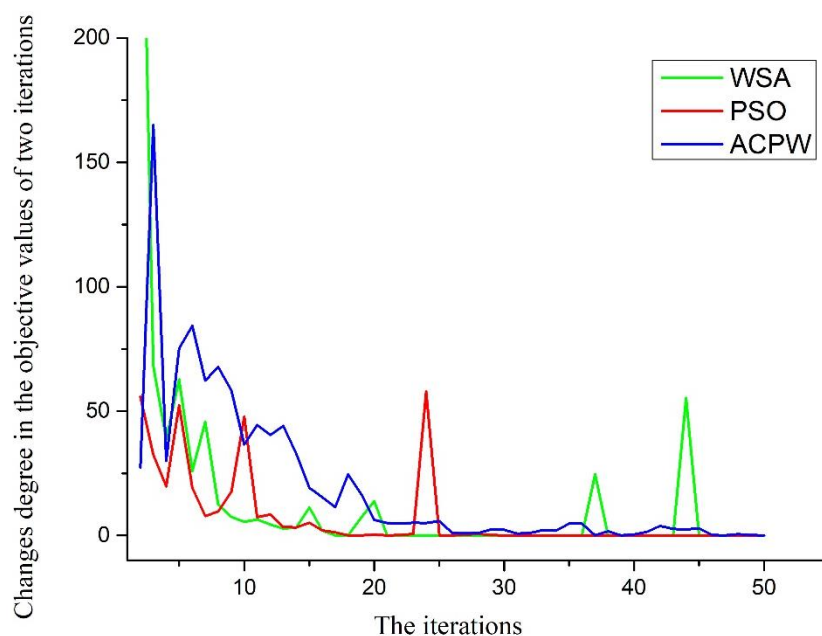


Figure 4: The changing degree of the PSO, WSA and ACPW methods. PSO is denoted as the red line, the WSA is shown as the green line, and the ACPW algorithm is represented as the blue line.

In Fig. 4, the change value is calculated from the subtraction of two objective values, e.g. the objective value of the second iteration minus the first objective value is the first change value. Obviously, the ACPW algorithm is continuously changing. The PSO algorithm often falls into a local optimum, which the change value is 0. The WSA has the stronger ability to escape a local optimum, although it also falls into a local optimum sometimes. Above all, we can conclude that the ACPW algorithm has better performance than the PSO and WSA, because we combine their strengths using hybrid strategy and cooperation co-evolution.”

A Novel Approach for Solving CNOPs and Its Application in Identifying Sensitive Regions of Tropical Cyclone Adaptive Observations

Linlin Zhang¹, Bin Mu¹, Shijin Yuan¹, Feifan Zhou^{2,3}

5 ¹School of Software Engineering, Tongji University, Shanghai 201804

²Laboratory of Cloud-Precipitation Physics and Severe Storms, Institute of Atmospheric Physics, Chinese Academy of Sciences, Beijing 100029

³University of Chinese Academy of Sciences, No.19 (A) Yuquan Road, Shijingshan District, Beijing 100049

Correspondence to: Shijin Yuan (yuanshijin2003@163.com)

10

Abstract. In this paper, a novel approach is proposed for solving conditional nonlinear optimal perturbations (CNOPs), called the “adaptive cooperation co-evolution of parallel particle swarm optimization and wolf (ACPW) search algorithm based on principal component analysis”. Taking Fitow (2013) and Matmo (2014) as two tropical cyclone (TC) cases, CNOPs solved by the ACPW algorithm are used to investigate the sensitive regions identified by TC adaptive observations with the fifth-generation mesoscale model (MM5). Meanwhile, the 60 km and 120 km resolutions are adopted. The adjoint-based method (short for the ADJ-method) is also applied to solve CNOPs, and the result is used as a benchmark. To evaluate the advantages of the ACPW algorithm, we run the PSO, WSA and ACPW programs 10 times and then compare the maximum, minimum and mean objective values as well as the RMSEs, and the analysis results prove that the hybrid strategy and cooperation co-evolution are useful and effective. To validate the ACPW algorithm, the CNOPs obtained from the different methods are compared in terms of the patterns, energies, similarities and simulated TC tracks with perturbations. (1) The ACPW algorithm can capture similar CNOP patterns as the ADJ-method, and the patterns of TC Fitow are more similar than TC Matmo. (2) At 120 km resolution, similarities between the CNOPs of the ADJ-method and the ACPW algorithm are higher than those at 60 km resolution. (3) Compared to the ADJ-method, although the CNOPs of the ACPW method produce lower energies, they can have improved benefits gained from the reduction of the CNOPs not only across the entire domain but also in the identified sensitive regions. (4) The sensitive regions identified by the CNOPs from the ACPW algorithm have the same influence on the improvements of the TC track forecast skills as those identified by the CNOPs from the ADJ-method. (5) The ACPW method has a higher efficiency than the ADJ-method. All conclusions prove that the ACPW algorithm is a meaningful and effective method for solving CNOPs and can be used to identify sensitive regions of TC adaptive observations.

15
20
25

1 Introduction

Tropical cyclones (TCs) are one of the most frequent and influential natural hazards in the world. An accurate forecast of TCs is conducive to the response of the government and people. Thus, it is essential to improve TC forecast skills. One effective way is to identify the sensitive regions of TC adaptive observations (TCAOs) (Franklin and Demaria, 1992; Bergot, 1999; Aberson, 2003). Once observations in sensitive regions are identified and added to reduce initial errors, better forecast will be expected (Bender et al., 1993; Zhu and Thorpe, 2006; Froude et al., 2007). Conditional nonlinear optimal perturbations (CNOPs) proposed by Mu and Duan (2003) are a nonlinear extension of the linear singular vector (SV) method and have been applied to study sensitive regions identification of TCAOs successfully (Mu and Zhou, 2009; Qin, 2010; Zhou and Mu, 2011, 2012a, 2012b; Zhou and Zhang, 2014; Qin and Mu, 2012; Qin et al., 2013; Qin and Mu, 2014; Wang et al., 2010; Wang et al., 2013).

Comparing between the sensitive regions identified from CNOPs and those identified through SVs, Qin (2010) concludes that the former is more appropriate for TCAOs. Zhou and Mu (2011) use the CNOP method to investigate different verification areas and how to affect the identification of sensitive regions. They also studied the influence of different horizontal resolutions (2012a). Moreover, different times and regime dependency was also researched (2012b). These research results directed further research. Zhou and Zhang (2014) propose three schemes for identifying sensitive regions based on the CNOP method and recommend the vertically integrated energy scheme. Moreover, some researchers analyse the sensitivity of dropwindsonde observations on TC predictions, which can be used in the CNOP method, and conclude that the sensitive regions identified by CNOPs have a positive impact on TC track predictions (Qin and Mu, 2012; Qin et al., 2013). In studies of improving the sensitivity of CNOPs in TC intensity forecasts, Qin and Mu (2014) suggest that the use of an ocean-coupled model needs to be considered as well as the better initialization of the TC vortex. Wang et al. (2013) use the CNOP method to study the mutual affection of binary typhoons. Previous studies have shown that the CNOP method is a useful and meaningful method for study the aforementioned phenomena (Zhou et al., 2013; Mu and Zhou, 2015).

There are generally two types of methods for solving CNOPs: one based on adjoint models (ADJ-method) and one without adjoint models. As useful and effective methods for solving CNOPs without adjoint models, some modified intelligent algorithms (IAs) based on dimension reduction have been successfully proposed and applied to solve CNOPs in the Zebiak-Cane (ZC) model, such as SAEP (simulated annealing based ensemble projecting method) (Wen et al., 2014), PPSO (principal component analysis) (PCA; Jolliffe, 1986)-based particle swarm optimization (Mu et al., 2015a), PCGD (principal components-based great deluge) (Wen et al., 2015a), RGA (robust PCA-based genetic algorithm) (Wen et al., 2015b), CTS-SS (continuous Tabu search algorithm with sine maps and staged strategy) (Yuan et al., 2015), and PCAGA (principal component analysis-based genetic algorithm) (Mu et al., 2015b). Compared to the ADJ-method, these methods all obtain CNOPs with similar spatial patterns and acceptable objective function values, and several of them have been paralleled with the message passing interface (MPI), reducing the computation time. In TC adaptive observations, such adjoint-free methods

are also required because the lack of adjoint models and solution spaces with too many dimensions have become obstacles for solving CNOPs; this is a focal point of this study.

We have adopted the PCAGA method to solve CNOPs for the sensitive regions identified by TCAOs with the fifth-generation mesoscale model (MM5) and obtained meaningful results (Zhang et al., 2017). However, we used a resolution of 120 km,

5 which is the lowest in such research. When using a higher resolution, more small-scale information can be predicted, and more accurate sensitive regions can be expected. It is necessary to use a higher resolution. Moreover, although the PCAGA method achieves meaningful results, its performance is not sufficient because it is based on a genetic algorithm, which has a good global searching ability but slow convergence rate. In addition, the PCAGA method was not parallelized in the previous study.

10 Therefore, in this paper, we propose a novel approach, adaptive cooperation co-evolution of PSO and wolf search algorithm (WSA) based on PCA (ACPW) to solve CNOPs for the sensitive regions identified by TCAOs. We take two tropical cyclones as study cases, Fitow (2013) and Matmo (2014), and simulate them with the MM5 model using two different resolutions, 60 km and 120 km. According to the study of Zhou and Zhang (2014), we adopt the total dry energy as the objective function. The CNOPs from the ADJ method are referred as a benchmark. Specific details of the ADJ-method can be found in Zhou (2009). To validate the ACPW method, the CNOPs from the ACPW method are compared with the benchmark in terms of the

15 patterns, energies, similarities and benefits from the CNOPs reduced in the entire domain and sensitive regions. Further, the CNOPs with different resolutions are also compared in terms of these aspects. To evaluate the sensitive regions located by the ACPW algorithm, we simulate TC tracks with the initial states perturbed by the amended CNOPs in the location of the sensitive regions from the ACPW algorithm and ADJ-method. Moreover, we design two schemes to amend the CNOPs: the same points and the equivalent proportional points. In addition, we evaluate the efficiency of the ACPW algorithm. All experimental results show that the ACPW method is a meaningful and effective method to solve CNOPs for selecting the sensitive regions of TCAOs.

The organization of the paper is as follows. Section 2 describes the formalized definition of CNOPs and the ACPW method. In section 3, we give the design of the experiments in this study. Section 4 presents the experimental analysis and results. Summaries and conclusions are provided in section 5.

25 2 Theory and Method

2.1 CNOPs

The mathematical formalism of CNOPs is described in Eq. (1). Under the constraint condition $\|u_0\|^2 \leq \delta$, an initial perturbation δu_0^* of vector U_0 (initial basic state) is called a CNOP if and only if

$$J(\delta u_0^*) = \max_{\|u_0\|^2 \leq \delta} J(u_{NT}), \quad (1)$$

30 where

$$u_{NT} = PM(U_0 + \delta u_0) - PM(U_0), \quad (2)$$

and P represents a local projection operator; the value within the verification region is 1 and 0 elsewhere.

$$U_t = M_{t_0 \rightarrow t}(U_0), \quad (3)$$

where M expresses a nonlinear propagation operator, and U_t is the development of U_0 at time t .

2.2 ACPW method

5 In this paper, we propose the ACPW method to solve CNOPs for identifying sensitive regions of TCAOs. The core of this approach is the cooperation co-evolution of two intelligent algorithms: PSO and WSA, and the adaptive number of two subswarms. PSO is a classical population-based stochastic optimization technique developed by Eberhart and Kennedy (1995) and inspired by social behaviours of bird flocking or fish schooling; it has been successfully and effectively applied to solve CNOPs in the ZC model for studying El Niño-Southern Oscillation (ENSO) predictions (Mu et al., 2015a). The WSA is a new
10 bio-inspired heuristic optimization algorithm based on wolf preying behaviours, which was proposed by Rui Tang et al. (2012) and has been applied to study the travelling salesman problem with test functions. Their experiments showed that the WSA is an effective global optimizing algorithm but requires long computation times.

We have adopted PSO and the WSA method to solve CNOPs in the MM5 model, although the results exhibit slow convergence or premature convergence. Hence, we combine the advantages of these two algorithms. We use the WSA to explore the global
15 space due to its independence and use PSO to examine the local space and ensure the convergence of the ACPW algorithm. Moreover, we design the adaptive subswarms of PSO and WSA for cooperation co-evolution. The ACPW framework is shown in Fig. 1.

In Fig. 1, the most important part of the ACPW algorithm is inside the dotted box. We divide the entire initial swarm into two subswarms with the same number of individuals: one updates the individuals with the PSO's rule and the other with the WSA's
20 rule. Then, the two subswarms are adaptively varied along with the convergence state of the ACPW algorithm, i.e., when the change in the objective function adaptive value is less than a threshold value, the number of individuals in the subswarm belonging to the WSA is increased, and the other subswarm belonging to PSO is decreased by an equal number of individuals to keep the same number for the entire swarm. ~~These improvements bring better convergence accuracy and higher evolution velocity, which is shown in Fig. 2.~~ The more specific analysis of the ACPW algorithm is discussed in section 4.

25 The process of solving CNOPs with the ACPW algorithm is described as follows:

- 1) *Randomly generate an initial swarm with N individuals.* An individual u_i needs to satisfy the boundary constraint in the terms of Eq. (4). Once u_i goes beyond the boundary, it must be pulled back, i.e.,

$$u_i = \begin{cases} u_i & \|u_i\| \leq \delta \\ \frac{\delta}{\|u_i\|} \times u_i & \|u_i\| > \delta \end{cases} \quad i = 1, \dots, N \quad (4)$$

- 2) *Divide the entire initial swarm into two subswarms with an adaptive coefficient α .* One subswarm updates individuals
30 with the PSO's rule and the other with the WSA's rule.
- 3) *Calculate the adaptive value of the objective function in parallel, i.e., $J(u_i)$ in Eq. (1).*

4) Update individuals by PSO (Eq. (5)) or the WSA (Eq. (6)).

$$\begin{cases} v_i^{k+1} = \omega v_i^k + c_1 \alpha (o_i^k - u_i^k) + c_2 \beta (o_g^k - u_i^k) \\ u_i^{k+1} = u_i^k + \gamma v_i^{k+1} \end{cases} \quad (5)$$

where the superscript k or $k + 1$ is the iterative step, v_i^{k+1} is the velocity of the individual u_i^k and calculated by the first subformula, ω is the inertia coefficient, c_1 and c_2 are the learning factors, α and β are the random numbers uniformly distributing on the interval from 0 to 1, o_i^k is the local optimum, o_g^k is the global optimum in the k^{th} iteration, γ is the restraint factor to control the speed, and u_i^{k+1} is the updated individual based on PSO.

There are two ways for updating individuals in the WSA, i.e., prey and escape, which represent the functions of searching in a local region and escaping from a local optimum:

$$\begin{cases} u_i^{k+1} = u_i^k + \theta \cdot r \cdot rand() \quad \text{Prey} \\ u_i^{k+1} = u_i^k + \theta \cdot s \cdot escape() \quad \text{Escape} \end{cases} \quad (6)$$

where the superscript k or $k + 1$ is also the iterative step, θ is the velocity, r is the local optimizing radius, which is smaller than the global constraint radius δ , $rand()$ is the random function, whose mean value is distributed in $[-1,1]$, $escape()$ is the function for calculating a random position, which is 3 times larger than r , and s is the step size of the updating individual.

As described in Eq. (6), the wolf has two behaviours, i.e., prey and escape. The prey behaviour uses the first sub-formula, and the second one is for the escape function, which happens in every iteration when the condition $p > p_a$ is satisfied, where p is a random number in $[0,1]$, and p_a is the probability of individual escaping from the current position.

5) Judge whether the change in the adaptive value of the objective function is smaller than ε . If yes, set a new value to the adaptive subswarm coefficient α . If not, continue running the process. The detailed updating procedure for α is described as follows:

$$\alpha = \begin{cases} \alpha + 0.05, & \text{if the bestvalue} - \text{current value} < \varepsilon \\ \alpha - 0.05, & \text{else} \end{cases} \quad (7)$$

In this paper, before we update the individuals, α is calculated, and then we divide the entire initial swarm into two subswarms according to the α value, i.e., the number of individuals depending on the PSO's rule is $\alpha \times N$, and the other number is $(1 - \alpha) \times N$. We set the initial value of ε and α to 0.1 and 0.5, respectively.

6) Judge whether the termination condition is satisfied. If yes, terminate the iteration. Otherwise, go to step 2.

All of above processes are based on the dimension reduction within PCA, whose procedure has been described in the study of Mu et al. (2015a). After many experiments, the parameters of the ACPW algorithm can be set, as shown in Table 1.

Although the parameters are more than for each single algorithm, most retain the empirical value of each algorithm and do not require adjustments. The reason for using a different number of individuals is that the internal storage memory was not sufficient when using more than 200 individuals, resulting in premature termination of the ACPW algorithm.

3 Experiments Design

All the experiments are run on a Lenovo Thinkserver RD430 with two Intel Xeon E5-2450 2.10 GHz CPUs, 32 logical cores and 132G RAM. And the operating system is CentOS 6.5. All the codes are written in FORTRAN language and compiled by PGI Compiler 10.2.

5 3.1 The model and Data

In this paper, we adopt the MM5 model to study the sensitive region identification of TCAOs, and the corresponding adjoint system of the MM5 model (Zou et al., 1997) is used to obtain the benchmark. The ERA interim daily analysis data ($1^\circ \times 1^\circ$) (Dee et al., 2011) from the European Center for Medium range Weather Forecasts (ECMWF) are used to generate the initial and boundary conditions. The physical parameterization schemes are defined as follows: dry convective adjustment, the high-resolution planetary boundary layer scheme, grid-resolved large-scale precipitation and the Kuo cumulus parameterization scheme.

We also utilize the best TC track data (Ying et al., 2014) from the China Meteorological Administration - Shanghai Typhoon Institute (CMA-SHTI) as TC tracks observed for evaluating the simulation TC tracks of the MM5 model.

3.2 Typhoons Fitow (2013) and Matmo (2014)

15 TCs Fitow (2013) and Matom (2014) are taken as the study cases and introduced below. Fitow was the 23rd TC in 2013 and developed to the east of the Philippines on 29 September, striking China at Fuding in Fujian Province on 6 October. Matom was the 10th named typhoon in 2014, and it formed on 17 July and made landfall in Taiwan on 22 July. For these two cases, 24 h control forecasts are set as background fields based on integration from 0000 UTC 5 Oct 2013 to 0000 UTC 6 Oct 2013 (TC Fitow) and from 1800 UTC 21 Jul 2014 to 1800 UTC 22 Jul 2014 (TC Matom). After the 24 h period, TC Fitow had a maximum sustained wind of 162 kilometres per hour, whereas TC Matmo had a maximum wind speed of 151.2 kilometres per hour. In addition, the forecasts were executed at 60 km and 120 km resolutions with 11 vertical levels, and the model domain covered 55×55 and 21×26 grids, respectively.

The simulated TC tracks from the MM5 model for these two cases are acceptable, as has been shown in our previous study (Zhang et al. 2017). The following analysis is based on those simulations.

25 3.3 Experimental setup

Because slight changes in the verification area never hurts the results (Zhou and Mu, 2011), we design the verification areas as rectangles covering the potential typhoon tracks at the forecast time.

The initial perturbation sample δu_0 is composed of the perturbed zonal wind u'_0 , meridional wind v'_0 , temperature T'_0 and surface pressure p'_{s0} . Each component can be represented as a $m \times n \times l$ matrix, where $m \times n$ is the distribution of the horizontal grid, and l denotes the number of vertical levels. To extract features for reducing the dimensions and solving CNOPs,

the $m \times n \times l$ matrix is reshaped to a $k \times 1$ vector, where $k = m \times n \times l \times S$ (S is the number of the components). Assuming we have R vectors to represent the features of the solution space, we recombine the R vectors to a $k \times R$ matrix and use PCA to capture the feature space with lower dimensions. Then, the CNOP is solved in the feature space until we obtain the global CNOP, which will be projected to the original solution space. When using the ACPW algorithm to solve CNOPs, its initial

5 inputs are produced by the random way in the feature space, and the CNOP has the largest nonlinear evolution at prediction time, i.e., the largest adaptive value of the objective function in Eq. (9). The objective function is measured by the total dry energy (Zhou and Zhang, 2014) because Dr. Zhou has proved that the sensitive regions gained by the dry energy have higher benefits than those obtained from the moist energy (Zhou, 2009).

The following is defined:

$$10 \quad f(i, j) = \int_0^1 E_T(i, j, \sigma) d\sigma, \quad (8)$$

where $E_T(i, j, \sigma)$ denotes the total dry energy of the CNOP at the MM5 grid point (i, j, σ) .

Corresponding to formula (1) and (2), we have

$$(u_{NT}) = \frac{1}{D} \int_D \int_0^1 \left[u_t'^2 + v_t'^2 + \frac{c_p}{T_r} T_t'^2 + R_a T_r \left(\frac{p_{st}}{p_r} \right)^2 \right] d\sigma dD, \quad (9)$$

where u_t' , v_t' , T_t' , and p_{st}' are the components of u_{NT} , which is the nonlinear development of the perturbed U_0 (i.e., $U_0 + \delta u_0$)

15 from the initial time t_0 to the prediction time t , and σ is the vertical coordinate. Table 2 illustrates the other reference parameters.

For the convenience of optimization, solving CNOPs can be transformed to a minimum problem as follows:

$$J(\delta u_0^*) = \min_{\|u_0\|^2 \leq \delta} \left(-\frac{1}{D} \int_D \int_0^1 \left[u_t'^2 + v_t'^2 + \frac{c_p}{T_r} T_t'^2 + R_a T_r \left(\frac{p_{st}}{p_r} \right)^2 \right] d\sigma dD \right). \quad (10)$$

To facilitate understanding, all symbols are listed in Table 2, and their meanings are also explained.

20 4. Experimental Results and Analysis

To evaluate the advantages of the ACPW algorithm, we run the PSO, WSA and ACPW programs 10 times and then compare the maximum, minimum and mean objective values as well as the RMSE. [We also exhibit the objective value scope after the first iteration to analyse the effect of initial objective values on the different algorithms. Meanwhile, to illustrate the performance of the algorithms, we compare the changing degree of the objective function value for the three algorithms.](#)

25 4.1 The advantages of the ACPW algorithm

Because the statistical analysis results are similar for the two TCs with the two resolutions, we only describe the analysis of Fitow at a resolution of 60 km. Table 3 presents the maximum objective value, the minimum objective value, the mean objective value and the RMSE of the 10 results.

In Table 3, the maximum objective value is gained from the ACPW algorithm, and its mean value is also more than the other two algorithms. However, the RMSE of PSO is the smallest, which shows the best stability.

For additional analysis, we draw a box-plot of the 10 results for the PSO, WSA and ACPW algorithms, as shown in Fig. 32. PSO has the narrowest range of values, although the objective values are smaller than the other two algorithms. The WSA has the widest range of values, although the objective values are also smaller than the ACPW algorithm. The ACPW algorithm has the second-best stability, although it has the best objective values. The experiments display the stability of PSO and the exploitation of the WSA. We combine the advantages of them and develop the ACPW algorithm to solve CNOPs. The analysis results demonstrate that the hybrid strategy and cooperation co-evolution is useful and effective.

Since these three algorithms are all heuristic algorithms with randomness, and the initial inputs are generated by random way, the initial objective value is different for every running. To analyse the effect of initial objective values on the different algorithms, we exhibit the objective value scope of the PSO, WSA and ACPW algorithms after the first iteration in Fig. 3.

In Fig. 3, for convenience, only integer is indicated in the coordinate system. In 10 experiments, the PSO has the narrowest scope from 467.1719 to 781.6482. The WSA and ACPW algorithms have similar value spans, which are wider than the PSO, but the objective values of the ACPW are higher. And the value scope is reasonable according to the characteristic of these three algorithms. The WSA has the strongest randomness, the PSO is the most stable, and the ACPW combines the advantages of the two. From the results, we cannot find the direct relationship between the initial objective value and the final result, but a better first objective value has a beneficial effect on finding the optimal value.

To illustrate better performance of the ACPW algorithm, we calculate the average objective value of every step of 10 program results, and then obtain the change degree between the two iterations. We draw them in Fig. 4. If the objective value is continuously changing, then the algorithm has better global searching ability; otherwise the algorithm tends to fall in local optimization.

In Fig. 4, the change value is calculated from the subtraction of two objective values, e.g. the objective value of the second iteration minus the first objective value is the first change value. Obviously, the ACPW algorithm is continuously changing. The PSO algorithm often falls into a local optimum, which the change value is 0. The WSA has the stronger ability to escape a local optimum, although it also falls into a local optimum sometimes. Above all, we can conclude that the ACPW algorithm has better performance than the PSO and WSA, because we combine their strengths using hybrid strategy and cooperation co-evolution.

4.2 CNOP patterns

To validate the ACPW algorithm for solving CNOPs and to identify the sensitive regions, we compare the ADJ-method and the ACPW algorithm results in terms of the CNOP patterns, energies, similarities, benefits from reduction of the CNOPs, and simulated TC tracks with perturbations.

In this subsection, we compare the CNOPs obtained from the ADJ-method and the ACPW algorithm in terms of the patterns of temperature and wind. Experimental results show that TC Fitow has more similar CNOP patterns than TC Matmo. The CNOP patterns are described in [Fig. 4Fig. 5](#).

At 120 km resolution for TC Fitow ([Fig. 4Fig. 5a, b](#)), the two methods have nearly the same major warm locations and similar cold regions, while the wind vectors have opposite directions. The ADJ-method captures the CNOP with two major locations. The red (warm) one is distributed to the west of the initial cyclone (IC), and the green (cold) one is distributed to the north of the IC. The ACPW algorithm also captures the CNOP with two main locations. The warm one is distributed to the west, and the cold one is located at the northwest of the IC. In this subsection, the spatial orientation is relative to the position of the IC. Therefore, in the following discussion, we explain the spatial orientation in the figures without repeating the IC.

For TC Fitow with a 60 km resolution ([Fig. 4Fig. 5c, d](#)), the CNOP spatial distribution based on the ACPW algorithm is very similar to the ADJ-method's results. In the northwest of the verification area, the two CNOPs have two similar major parts, one warm area and one cold area. The difference between these two patterns is that the ADJ-method has another major warm area located in the northwest, while the ACPW method produces another major warm area in the east. The distribution of the secondary parts exhibits only a slight difference.

For the same method with the different resolutions ([Fig. 4Fig. 5a, c](#) and [Fig. 4Fig. 5b, d](#)), the CNOP patterns have similar major distributions in the northwest, although within a different region. The reason is that when using a higher resolution, more small-scaled phenomena can be resolved (Zhou and Mu, 2012a).

For TC Matmo with a 120 km resolution ([Fig. 5Fig. 6a, b](#)), the ADJ-method and ACPW algorithm obtain CNOPs with different spatial patterns in terms of temperature and wind. The ADJ-method has two major parts, with the warm one located in the west and the cold one in the east. The ACPW algorithm results in two main parts distributed in the northeast with one warm area near the IC and a cold one far from the IC. For TC Matmo with a 60 km resolution ([Fig. 5Fig. 6c, d](#)), in the verification area, the two CNOP patterns have similar spatial distributions, with two warm areas located at nearly the same positions. However, the parts outside the verification area are distributed in different locations. Moreover, the CNOP of the ADJ-method has more regular distributions than the ACPW's distributions. For the same method with different resolution ([Fig. 5Fig. 6a, c](#) and [Fig. 5b6b, d](#)), the CNOP patterns cover similar areas but with different ranges and details.

Based on the above analysis regarding the patterns of temperature and wind, we can conclude that when using a resolution of 60 km, the CNOPs predicted by the ADJmethod and ACPW algorithm have more similar major patterns than those predicted at a resolution of 120 km. In addition, the ACPW algorithm can obtain CNOPs with more similar patterns in TC Fitow than in TC Matmo.

Vertically integrated energies of the CNOPs for TC Fitow are displayed in [Fig. 6Fig. 7](#). Compared to the ADJ-method, at 120 km resolution, the CNOPs of the ACPW method have much lower energy and differing positions. However, when using a resolution of 60 km, similar energies and positions are obtained. Moreover, the energy of the CNOPs obtained from the ACPW algorithm has a larger range in the centre.

Vertically integrated energies of the CNOPs for TC Matmo are displayed in Fig. 7 Fig. 8. Compared with the ADJ-method, at 120 km resolution, the CNOPs of the ACPW algorithm have a lower energy and cover larger areas. However, when using a resolution of 60 km, although the energy is still lower, the positions are more similar.

4.2 Similarities

5 When we evaluate the CNOPs, in addition to the characteristics and distributions of the CNOP patterns, consideration should also be given to numerical similarities and to the benefits of the CNOPs. Therefore, we calculate the similarity between the CNOPs determined from the ADJ-method and the ACPW algorithm and use X and Y to represent them in formula (10).

$$S_{xy} = \frac{\langle X, Y \rangle}{\sqrt{\langle X, X \rangle} \sqrt{\langle Y, Y \rangle}} \quad (10)$$

10 The results are shown in Table 4. The similarity values can reflect the similarities among the CNOP patterns (Fig. 4 Fig. 5 and Fig. 5 Fig. 6).

In Table 4, for TC Fitow, the similarity at 120 km is -0.83, whereas that with a resolution of 60 km is 0.43. For TC Matmo, the similarity at 120 km is 0.42, whereas that with a resolution of 60 km is 0.37. The negative sign indicates that portions of the CNOPs from these two methods have opposite wind vector directions, which is shown in Fig. 4 Fig. 5. We also find that when using a higher resolution, the similarity is lower. The reason for this finding is that although the major patterns of the CNOPs are similar, the secondary parts differ and they cover larger areas. When using a higher resolution, we can achieve more small-scale information, and the identification of sensitive regions becomes more accurate. Regarding the analysis of the CNOP patterns, we obtain more similar major patterns when for a resolution of 60 km resolution. However, compared with the other different parts, the similar parts are very small. The decreased similarities decreased do not affect identifying the sensitive regions because the adaptive observations only focus on the points with larger influences, which will be demonstrated subsection 4.4.

20 We also compare the energy for 24 hours of nonlinear development under the initial states perturbed by different CNOPs, i.e., $J(M(U_0 + \delta u_0^*))$. The results are shown in Table 5. All CNOPs obtained using the ACPW produce lower energies than the those of the ADJ-method. However, when reducing the CNOPs to $W \times$ CNOPs in the entire domain and reducing the CNOPs by a factor of 0.5 in the sensitive regions, the ACPW algorithm has better results, which will be discussed in following subsection.

4.3 Benefits from Reducing the CNOPs

In this subsection, we design two groups of idealized experiments to investigate the validity of the sensitive regions identified using CNOPs based on the following assumptions:

30 When adding adaptive observations in sensitive regions, the surrounding environment is idealized, and the improvements from adding observations reduces the original errors by a factor of 0.5.

The obtained CNOPs can be seen as the optimal initial perturbations. Once we reduce them in the sensitive regions, the benefits are highest.

Under these assumptions, by reducing the CNOPs to $W \times$ CNOPs and inserting them into the initial states we can investigate how the reductions in the CNOPs influence TC forecast skill. Moreover, reducing the CNOPs by a factor of 0.5 in the identified sensitive regions by vertically integrated the energies can be used investigate how the addition of adaptive observations in the sensitive regions can impact TC forecast skill.

First, because CNOPs can be seen as the optimal initial perturbations in the TCAOs, we reduce the CNOPs to $W \times$ CNOP, where W is a coefficient in (0, 1), and insert the reduced CNOPs into the initial state and allow for 24 h of evolution of the MM5 model. Then, we calculate the forecast error using formula (11) to determine the benefits of the reductions. Second, we determine the sensitive regions via vertically integrated energies using two schemes: the same points in the different resolutions and the equivalent percentage of points from the different grids. Then, we reduce the CNOPs by a factor of 0.5 only in the sensitive regions and insert the amended CNOPs into the initial states. The model is run for 24 h. The experimental results are described below.

4.3.1 Reducing the CNOPs to $W \times$ CNOPs in the entire domain

We explore the forecast improvements induced by reducing the CNOPs to $W \times$ CNOPs for the entire domain. The approach requires using the reduced CNOPs in the initial state for a 24-h simulation of the MM5 model. The prediction error is computed by formula (11):

$$J_1(u_{NT}) = \|PM(U_0 + \delta u_0) - PM(U_0)\|^2, \quad (11)$$

where the definitions of u_{NT} , P , M and U_0 are the same as in Eq. (1), (2) and (3).

The prediction error after reducing the CNOPs for the entire domain is computed by formula (12):

$$J_2(u_{NT}) = \|PM(U_0 + W\delta u_0) - PM(U_0)\|^2, \quad (12)$$

where W is the weighting coefficient, which is set to 0.25, 0.5 or 0.75 for decreasing error. The benefit from such reductions is calculated by formula (13):

$$\frac{J_1(u_{NT}) - J_2(u_{NT})}{J_1(u_{NT})}. \quad (13)$$

The prediction benefit increases for decreasing W . [Fig-8Fig. 9](#) and [Fig-9Fig. 10](#) also show that the ACPW algorithm can obtain CNOPs with better benefits from reducing the CNOPs to $W \times$ CNOPs for the entire domain than the ADJ-method except for when W is 0.25 for TC Fitow at a resolution of 60 km. This is because the ACPW algorithm optimizes a low-dimensional feature space due to the PCA and focuses on more effective points in the entire domain, which has positive effects on improving the forecast.

4.3.2 Reducing the CNOPs by a factor of 0.5 in the sensitive regions

We explore the forecast improvement caused by reducing the CNOPs by a factor of 0.5 in the sensitive regions. We determine the sensitive regions based on vertically integrated energies using two schemes: the 20 points with the highest energy at the different resolutions and 1/100 points of the different grids, which is 30 points at 60 km resolution (55×55) and 6 points at 120 km resolution (21×26). The sensitive regions with the 20 points having the highest energy are denoted in [Fig. 10](#)[Fig. 11](#) and [Fig. 11](#)[Fig. 12](#).

In [Fig. 9-10](#) and [Fig. 10](#)[Fig. 11](#), when the equivalent points approach is adopted, a larger scope is covered with 120 km resolution than with 60 km resolution. When using the 20 points from the ADJ-method and ACPW algorithm and reducing the CNOPs by a factor of 0.5, the benefits are displayed in Table 6.

In Table 6, for TC Fitow, compared to the ADJ-method, i.e., 5.93% at 120 km resolution and 3% at 60 km resolution, the ACPW algorithm obtains a higher benefit (8.05%) for a resolution of 120 km and a lower benefit (-0.84) for a resolution of 60 km. Here, -0.84% means that a reduction in the CNOPs results in no benefit and narrows the quality of the initial state. For TC Matmo, the ACPW algorithm achieves a much higher benefit (20.48%) than the ADJ-method (6.12%) at 60 km resolution, while a lower benefit (16.26%) than the ADJ-method (20.90%) at 120 km resolution. In addition, when using the same number of energy points, the benefits using 120 km resolution are nearly as high as those for 60 km resolution except for the ACPW algorithm at 60 km resolution for TC Matmo.

The sensitive regions with 1/100 points from the different grids are denoted in [Fig. 12](#)[Fig. 13](#) and [Fig. 13](#)[14](#).

[Fig. 12](#)[Fig. 13](#) and [Fig. 13](#)[14](#) show that when using different resolutions, the sensitive regions identified by the same method are different. The sensitive regions identified by the ACPW algorithm are more dispersive than those identified by the ADJ-method, which is attributed to randomness of the intelligent algorithms. Table 7 shows the benefits gained from reducing the CNOPs by a factor of 0.5 in the sensitive regions identified by the ADJ-method and ACPW algorithm with different points in the different resolutions.

According to Table 7, for TC Fitow, the ACPW algorithm achieves a 4.23% benefit, which is higher than the ADJ-method (3.9%) at 60 km resolution and a lower benefit 0.01% than the ADJ-method (1.72%) at 120 km resolution. For TC Matmo, the ACPW algorithm also has a higher benefit (9.75%) and a lower benefit (6.86%) than the ADJ-method (1.21% and 13.24%, respectively).

Combined with Table 6 and Table 7, we can conclude that the sensitive regions cover a larger scope, and higher benefits are obtained. When using the same proportion of grids with the different resolutions, the sensitive regions under higher resolution achieve higher benefits. These results also demonstrate that the CNOPs obtained from the ACPW algorithm can identify sensitive regions with higher benefits at 60 km resolution.

4.4 Simulated TC Tracks

We further investigate the validity of the sensitive regions identified by the CNOPs using a comparison of simulated TC tracks predicted by the MM5 model for each case by inserting the CNOPs or W×CNOPs into the initial states; we also simulate the TC tracks by inserting amended CNOPs in the different sensitive regions (20 or 30 points). Because 120 km is the lowest resolution in this research and the tracks cannot be drawn under this resolution in our study, we only analyse the simulated TC tracks at 60 km resolution. We draw two tracks in a subfigure, which are the observed TC track from the CMA-SHTI and the simulated TC track from the MM5 model; the different perturbations are overlaid onto the same initial states. According to the experimental results, when overlaying the CNOPs or amended CNOPs onto the same initial states, although the CNOPs are obtained from different methods, the simulated tracks are the same. Therefore, we only discuss one group of figures for each case. The results are presented in [Fig. 44-15](#) and [Fig. 45-16](#).

[Fig. 44-15](#) demonstrates the simulated TC tracks of the MM5 by inserting the CNOPs or W×CNOP into the initial state for TC Fitow; the four subfigures are the same. The reason is that the deviations between the simulated TC track and the observed TC track are very small; it is not easy to make improvements. Hence, when inserting different CNOPs into identical initial states to simulate TC tracks, a change is not evident. Moreover, the resolution we used was 60 km, which is not high enough to show more details about changing tracks.

[Fig. 45-16](#) demonstrates the simulated TC tracks from the MM5 model by inserting the CNOPs or W×CNOP into the initial state for TC Matmo. Subfigures (a) and (b) are the same, and from (b) to (d), the simulated positions after 24 hours are getting closer to the observed positions. These results illustrate that when the CNOPs obtained by the ACPW algorithm and ADJ-method are used as the optimal initial perturbations, reducing the CNOPs has a positive effect on the forecast skill of the simulated tracks. Moreover, the ACPW algorithm is a meaningful and effective method for solving the approximate CNOPs of the ADJ-method.

We also simulate TC tracks by inserting the amended CNOPs, which are reduced by a factor of 0.5 in only the sensitive regions. We use 20 and 30 points as the sensitive regions to study how the number of points affects the forecast skill. The results are shown in [Fig. 46-17](#) and [Fig. 47-18](#).

In [Fig. 46-17](#) and [Fig. 47-18](#), the simulated TC tracks are the same for not only different methods but also different sensitive regions. We can conclude that the ACPW algorithm, an adjoint-free method, is a meaningful and effective method for solving the approximate CNOPs of the ADJ-method. According to these results, we can also conclude that using 20 or 30 points as the sensitive regions results in the same improvement in the TC tracks in terms of forecast skill. Thus, fewer points can be used in real adaptive observations to reduce costs.

4.5 The efficiency of the ACPW algorithm

To promote the efficiency of the ACPW algorithm, we parallelize it with MPI technology. The time consumption of each case is nearly the same. Hence, we can use one group of experimental results to elucidate the efficiency of the ACPW algorithm.

Because the ADJ-method cannot be parallelized because each input depends on the output of the previous step, its time consumption is not changed. Moreover, because this method generally uses 4~8 initial guess fields to obtain the optimal value, we use one and four initial first guess fields to determine the CNOPs. The time consumptions of the ADJ-method and ACPW algorithm are shown in Table 8.

5 1. ADJ-method (1) means using 1 initial guess field and ADJ-method (4) means using 4 initial guess fields.

At 120 km resolution, the time consumptions of the ADJ-method using 1 and 4 initial guess fields are 12.4 minutes and 49.7 minutes, respectively. At 60 km resolution, the time consumptions are 79.9 minutes and 321.1 minutes, respectively. Unlike the ADJ-method, the ACPW algorithm can be parallelized. When using 22 cores, the ACPW method requires much less time, i.e., 2.74 minutes at 120 km resolution and 20.8 minutes at 60 km resolution. Obviously, the ACPW has higher efficiency.

10 Compared to the ADJ-method (1), the speedup reaches 4.53 and 3.84 for the different resolutions. Compared to the ADJ method (4), the speedup reaches 18.14 and 15.44. Although the different initial guess fields are calculated in parallel, the time consumption must be more than for the ADJ-method (1); the ACPW algorithm is also faster than the ADJ-method.

5 Summaries and Conclusions

In this study, we present a novel approach, adaptive cooperation co-evolution of paralleled PSO and WSA (ACPW), to solve
15 CNOPs. The CNOPs based on the ACPW algorithm are applied to study sensitive region identification in TCAOs in the MM5 model without using an adjoint model. We study two TC cases, Fitow (2013) and Matmo (2014), with 60 km and 120 km resolutions. The objective function is set as the total dry energy based on 24-hour simulations starting with initial perturbations at the prediction time within the verification area. We also calculate CNOPs with the ADJ-method; these results are used as a benchmark. To validate the ACPW algorithm, the CNOPs obtained from the different methods are compared in terms of the
20 patterns, energies, similarities, benefits of reduction of the CNOPs and simulated TC tracks with perturbations. To evaluate the advantages of the ACPW algorithm, we run the PSO, WSA and ACPW programs 10 times and compare the maximum, minimum and mean objective values as well as the RMSE; the analysis results demonstrate that the hybrid strategy and cooperation co-evolution are useful and effective.

According to all of the experiments, the following five conclusions are obtained:

25 (1) Compared with the ADJ-method, the ACPW algorithm can obtain CNOPs with more similar patterns of temperature and wind for TC Fitow than those for TC Matmo.

(2) At 120 km resolution, the similarities in the CNOPs achieved by the ADJ-method and the ACPW algorithm are higher than those at 60 km. The reason is that although the major patterns of the CNOPs are similar, the other parts differ and cover larger areas. At a higher resolution, we can resolve more small-scale information. Moreover, sensitive region identification becomes
30 more accurate. Regarding the CNOP patterns, more similar major patterns are obtained at 60 km resolution, although the similar parts are very small compared with the other differing parts. However, the decreased similarities do not affect identifying sensitive regions because the adaptive observations only focus on the points with a larger influence.

(3) When adding adaptive observations in the sensitive regions for a surrounding environment that is idealized, the original errors are reduced by a factor of 0.5; the CNOPs can be seen as the optimal initial perturbations. Once they are reduced in the sensitive regions, the benefits are highest. We design two groups of idealized experiments to investigate the validity of the sensitive regions identified by the CNOPs for TC track forecast skill: reducing CNOPs to $W \times$ CNOPs and reducing the CNOPs by a factor of 0.5 in the sensitive regions identified using vertically integrated energies. The experimental results show that the CNOPs of the ACPW algorithm produce lower energies than the ADJ-method but can obtain better benefits when reducing the CNOPs.

(4) The ACPW algorithm can be effective for identifying the sensitive regions, which have the same influence on the forecast improvements of the simulated TC tracks with the ADJ-method. We compare the different forecast improvements of the TC tracks from the different reduced perturbations, including reducing the CNOPs to $W \times$ CNOPs for the entire domain and reducing the CNOPs by a factor of 0.5 in the sensitive regions. The experimental results all support our conclusions.

(5) The ACPW algorithm has a higher efficiency than the ADJ-method. Compared to the ADJ method using 1 initial guess field, the speedup reaches 4.53 at 120 km resolution and 3.84 at 60 km resolution. Compared to the ADJ-method using 4 initial guess fields, the speedup reaches 18.14 and 15.44, respectively.

All of the conclusions demonstrate that the ACPW algorithm is a meaningful and effective method for solving approximate CNOPs and identifying sensitive regions of TCAOs. In addition, as we reduce the dimensions with PCA, the CNOPs obtained lose some energy. Compared to the CNOPs from the ADJ-method, the CNOPs from the ACPW algorithm are all local CNOPs. However, for the ACPW algorithm, they are global CNOPs. Because PCA makes our optimization focus on more effective points with higher energies, the ACPW algorithm can achieve the CNOPs with better benefits and the same improvements on TC track forecast skill.

We are restricted to computation resources for the time being. We are also limited by the parallelization of the ACPW algorithm. We will improve the computation conditions and use the parallel ACPW algorithm to solve CNOPs in the weather research forecast (WRF) model with a finer grid and higher resolution. In addition, we will apply this type of method to solve CNOPs in the community earth system model (CESM) model, which does not have an adjoint model.

Acknowledgments: In this paper, the research was sponsored by the Foundation of National Natural Science Fund of China (No.41405097).

References

- Aberson, S. D.: Targeted Observations to Improve Operational Tropical Cyclone Track Forecast Guidance, *Mon. Wea. Rev.*, 131(131), 1613, 2003.
- Bender, M.A., Ross, R.J., and Tuleya, R.E., Kurihara, Y.: Improvements in tropical cyclone track and intensity forecasts using the GFDL initialization system, *Mon. Wea. Rev.*, 121, 2046–2061, 1993.

- Bergot T.: Adaptive observations during FASTEX: A systematic survey of upstream flights, *Quart. J. Roy. Meteor. Soc.*, 125(561), 3271-3298, 1999.
- Dee, D. P., and 35 co-authors.: The ERA-Interim reanalysis: Configuration and performance of the data assimilation system, *Quart. J. Roy. Meteor. Soc.*, 137, 553-597, 2011.
- 5 Franklin, J. L., and Demaria, M.: The Impact of Omega Dropwindsonde Observations on Barotropic Hurricane Track Forecasts, *Mon. Wea. Rev.*, 120(120), 381-391, 1992.
- Froude, L. S. R., Bengtsson, L., Hodges, K. I.: The Predictability of Extratropical Storm Tracks and the Sensitivity of Their Prediction to the Observing System, *Mon. Wea. Rev.*, 135(2), 315-333, 2007.
- Jolliffe, I. T.: *Principal Component Analysis*, Springer Berlin, 87(100), 41-64, 1986.
- 10 Kennedy, J., and Eberhart, R.: Particle swarm optimization, in: *Proc. of IEEE Int. Conf. Neural Networks*, 1942-8, 1995.
- Mu, B., Wen, S., Yuan, S., and Li, H.: PPSO: PCA based particle swarm optimization for solving conditional nonlinear optimal perturbation, *Comput. Geosci.*, 83, 65-71, 2015a.
- Mu, B., Zhang, L., Yuan, S., and Li, H.: PCAGA: principal component analysis based genetic algorithm for solving conditional nonlinear optimal perturbation, in: *2015 International Joint Conference on Neural Networks (IJCNN)*, IEEE, Ireland, 12-17
- 15 July 2015, 1-8, 2015b.
- Mu, M., and Duan, W. S.: A new approach to studying ENSO predictability: Conditional nonlinear optimal perturbation, *Chinese Sci. Bul.*, 48, 1045-1047, 2003.
- Mu, M., and Zhou, F. F.: The Research Progress of the Typhoon Targeted Observations Based on CNOP Method, *Adv. Meteor. Sci. Technol.*, 3, 6-17, 2015.
- 20 Mu, M., Zhou, F., and Wang, H.: A Method for Identifying the Sensitive Areas in Targeted Observations for Tropical Cyclone Prediction: Conditional Nonlinear Optimal Perturbation, *Mon. Wea. Rev.*, 137(5), 1623-1639, 2009.
- Qin, X. H.: A Comparison Study of the Contributions of Additional Observations in the Sensitive regions Identified by CNOP and FSV to Reducing Forecast Error Variance for the Typhoon Morakot, *Atmos. & Ocean. Sci. Lett.* 03(05), 258-262, 2010.
- Qin, X., Duan, W., and Mu, M.: Conditions under which CNOP sensitivity is valid for tropical cyclone adaptive observations,
- 25 *Quart. J. Roy. Meteor. Soc.*, 139(675), 1544-1554, 2013.
- Qin, X., and Mu, M.: Can Adaptive Observations Improve Tropical Cyclone Intensity Forecasts?, *Adv. Atmos. Sci.*, 31(2), 252-262, 2014.
- Qin, X.H., and Mu, M.: Influence of conditional nonlinear optimal perturbations sensitivity on typhoon track forecasts, *Quart. J. Roy. Meteor. Soc.*, 662(138), 185-97, 2012.
- 30 Tang, R., Fong, S., Yang, X. S., and Deb, S.: Wolf search algorithm with ephemeral memory, in: *Seventh International Conference on Digital Information Management*, University of Macau, Macau, June 2012, 165-172, 2012.
- Wang, X. L., Zhou, F. F., and Zhu, K. Y.: The application of conditional nonlinear optimal perturbation to the interaction between two binary typhoons fengshen and fung-wong., *J. Trop. Meteorol.*, 29(2), 235-244, 2013.

- Wang, X., Zhum K., and Zhou, F.: The Study of Conditional Nonlinear Optimal Perturbation'S Application in Typhoon Over the South China Sea (in Chinese), *Tournal of Chengdu University of Information Technology*, 6(25), 640-646, 2010.
- Wen, S., Yuan, S., Mu, B., Li, H., and Chen L.: SAEP: Simulated Annealing Based Ensemble Projecting Method for Solving Conditional Nonlinear Optimal Perturbation, in: *Algorithms and Architectures for Parallel Processing*, 14th international conference, ICA3PP 2014, Dalian, China, 24–27 August 2014, 655-668, 2014.
- Wen, S., Yuan, S., Mu, B., Li, H., and Ren, J.: PCGD: Principal components-based great deluge method for solving CNOP, in: *Evolutionary Computation (CEC)*, 2015 IEEE Congress on. IEEE, 25-28 May 2015, 1513-1520, 2015a.
- Wen, S., Yuan, S., Mu B, and Li, H.: Robust PCA-Based Genetic Algorithm for Solving CNOP, in: *Intelligent Computing Theories and Methodologies*, 11th International Conference, ICIC 2015, Fuzhou, China, 20-23 August 2015, 597-606, 2015b.
- Ying, M., Zhang, W., Yu, H., Lu, X., Feng, J., Fan, Y., Zhu, Y., and Chen, D.: An overview of the China Meteorological Administration tropical cyclone database, *J. Atmos. Oceanic Technol.* (31), 287-301, 2014.
- Yuan, S., Qian, Y., and Mu, B.: Paralleled Continuous Tabu Search Algorithm with Sine Maps and Staged Strategy for Solving CNOP, in: *Algorithms and Architectures for Parallel Processing*, 15th International Conference, ICA3PP 2015, Zhangjiajie, China, 18-20 November 2015, 281-294, 2015.
- Zebiak, S.E., Cane, M.A.: A Model El Niño-Southern Oscillation. *Mon. Wea. Rev.*, 10(115), 2262-2278, 1987.
- Zhang, L. L., Yuan, S. J., Mu, B., and Zhou F. F.: CNOP-based sensitive areas identification for tropical cyclone adaptive observations with PCAGA method, *Asia-Pac. J. Atmos. Sci.*, 53(1), 63-73, 2017.
- Zhou Feifan. Application of conditional nonlinear optimal perturbation method to typhoon target observation. Institute of Atmospheric Physics, Chinese Academy of Sciences, 2009.
- Zhou, F., and Mu, M.: The impact of verification area design on tropical cyclone targeted observations based on the CNOP method, *Adv. Atmos. Sci.*, 28(5), 997-1010, 2011.
- Zhou, F., and Mu, M. The Impact of Horizontal Resolution on the CNOP and on Its Identified Sensitive Areas for Tropical Cyclone Predictability, *Adv. Atmos. Sci.*, 29(01), 36-46, 2012a.
- Zhou, F., and Mu, M.: The Time and Regime Dependencies of Sensitive Areas for Tropical Cyclone Prediction Using the CNOP Method, *Adv. Atmos. Sci.*, 29(04), 705-716, 2012b.
- Zhou, F., Qin, X., Chen, B., and Mu, M.: The Advances in Targeted Observations for Tropical Cyclone Prediction Based on Conditional Nonlinear Optimal Perturbation (CNOP) Method, in: *Data Assimilation for Atmospheric, Oceanic and Hydrologic Applications (Vol. II)*, Springer Berlin Heidelberg, 577-607, 2013.
- Zhou, F., and Zhang, H.: Study of the Schemes Based on CNOP Method to Identify Sensitive Areas for Typhoon Targeted Observations, *Chinese J. Atmos. Sci.* (2), 261-272, 2014.
- Zhu, H., and Thorpe, A. Predictability of Extratropical Cyclones: The Influence of Initial Condition and Model Uncertainties, *J. Atmos. Sci.*, 63(5). 1483-1497, 2006.
- Zou, X. F., Vandenbergh, M. Pondeva, and Kuo, Y-H.: Introduction to adjoint techniques and theMM5 adjoint modeling system, NCAR Tech. Note, NCAR/TN-435-STR, 107, 1997.

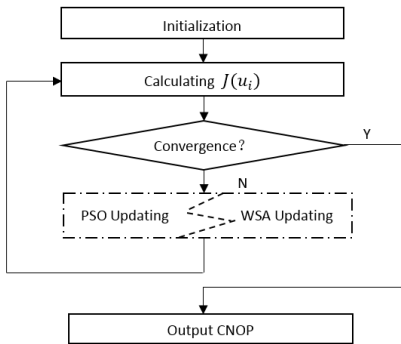
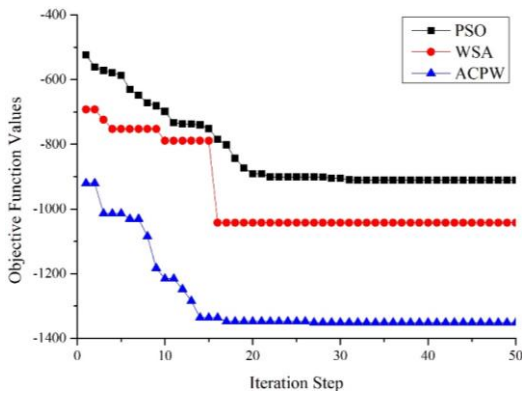


Figure 1:



5 Figure 2: Convergence of the PSO, WSA and ACPW methods. PSO is denoted as the black line with squares, the WSA is shown as the red line with circles, and the ACPW algorithm is represented as the blue line with triangles.

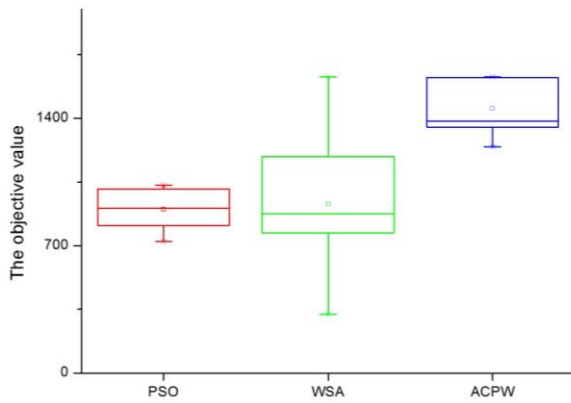


Figure-32: Box-plot of the PSO, WSA and ACPW methods for TC Fitow at 60 km resolution. The red box denotes PSO, the green box is for the WSA, and the blue box shows the results of the ACPW algorithm.

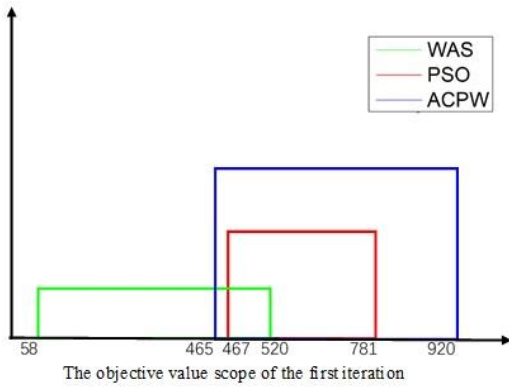


Figure 3: The first objective value scope of the PSO, WSA and ACPW methods. PSO is denoted as the red line, the WSA is shown as the green line, and the ACPW algorithm is represented as the blue line.

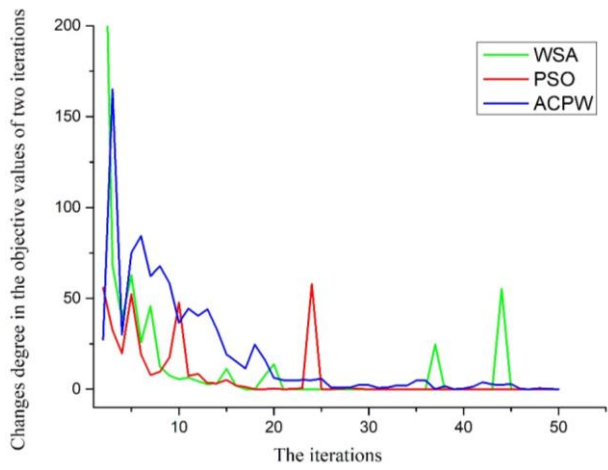


Figure 4: The changing degree of the PSO, WSA and ACPW methods. PSO is denoted as the red line, the WSA is shown as the green line, and the ACPW algorithm is represented as the blue line.

带格式的: 字体:(中文)+中文正文(宋体),(中文)中文(中国)

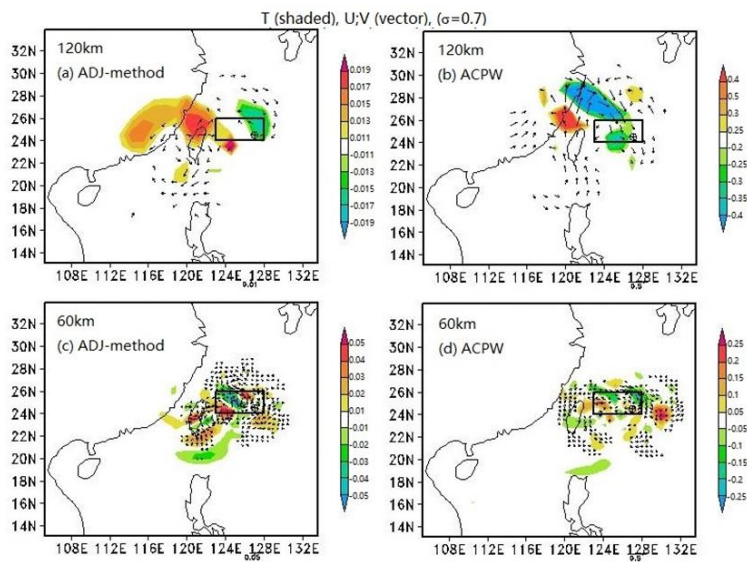


Figure 45: CNOP patterns at $\sigma=0.7$ for TC Fitw. The shaded parts represent temperature (units: K), and the vectors describe the wind (units: m s⁻¹). The squares indicate the verification areas, and the initial cyclone positions are shown by \oplus . (a) and (b) denote the CNOP patterns at 120 km resolution for the ADJ-method and ACPW algorithm, respectively; (c) and (d) represent the CNOP patterns at 60 km resolution for the ADJ-method and ACPW algorithm, respectively.

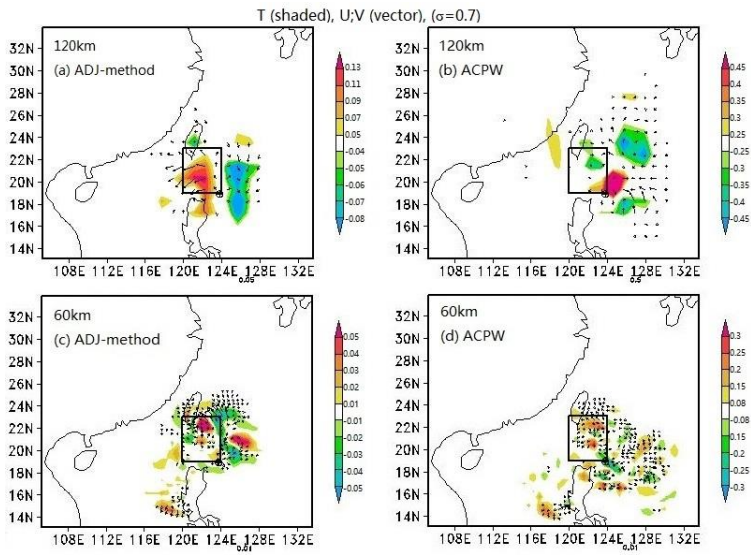


Figure 56: As in Fig. 3 except for tropical storm Matmo.

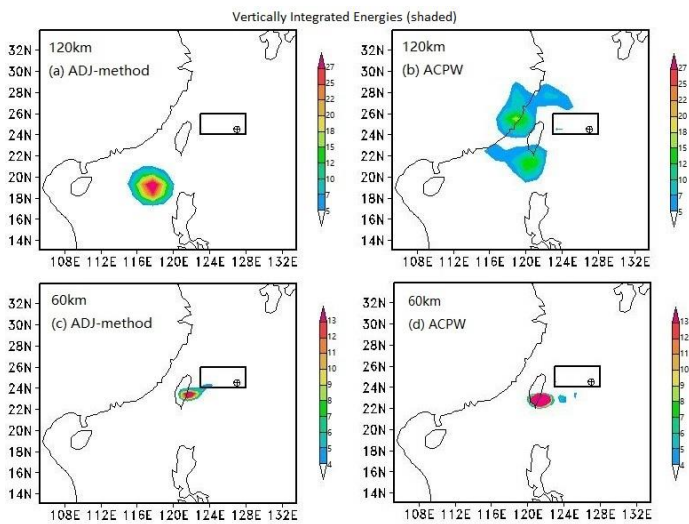


Figure 67: As in Fig. 3 except that the shaded parts represent the vertically integrated energies (units: J kg-1).

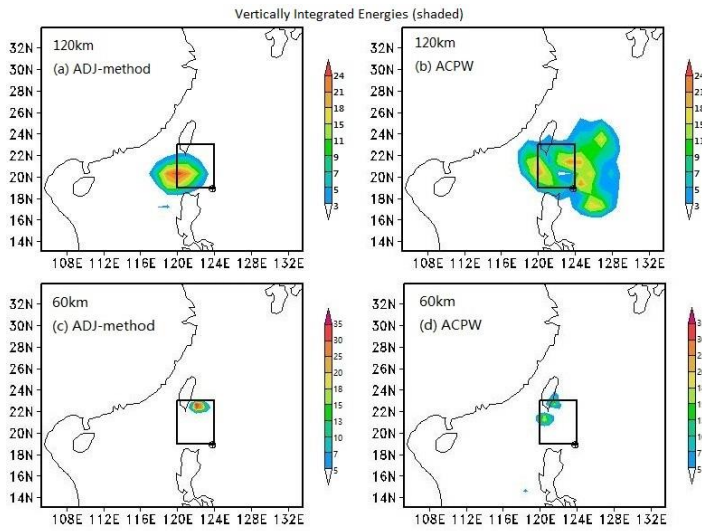
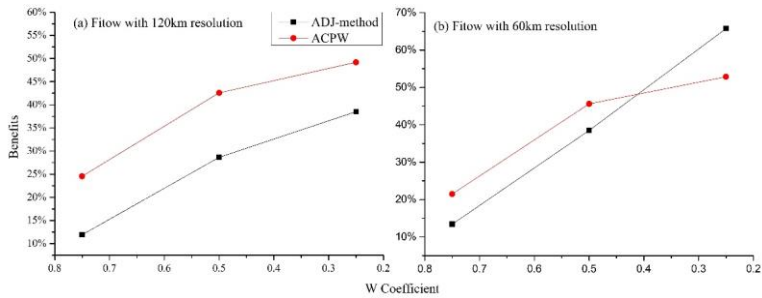


Figure 78: As in Fig. 4 Fig. 5 except that the shaded parts represent the vertically integrated energies (units: J kg-1).



5 Figure 89: Benefits (percent, %) gained from reducing the CNOPs to $W \times \text{CNOPs}$ for the ADJ-method and ACPW algorithm across the entire domain for TC Fitw (2013). The x-coordinate is the W coefficient values, and the y-coordinate denotes the benefits (percent, %) derived from the two methods. The ADJ-method is presented as the black line with squares, and the ACPW result is the red line with circles.

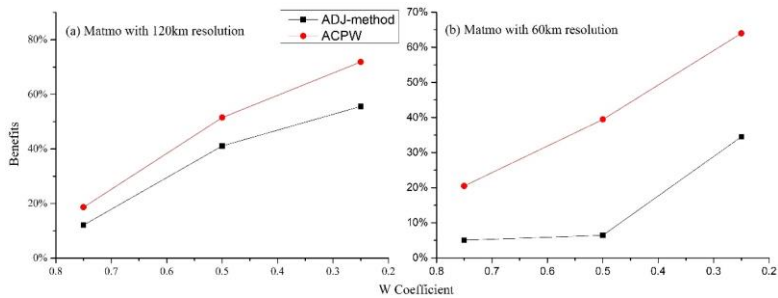


Figure 910: Benefits (percent, %) gained by reducing the CNOPs to $W \times$ CNOPs for the ADJ-method and ACPW algorithm across the entire domain for TC Matmo (2014). The x-coordinate is the W coefficient values, and the y-coordinate denotes the benefits (percent, %) derived from the two methods. The ADJ-method is presented as the black line with squares, and the ACPW result is the red line with circles.

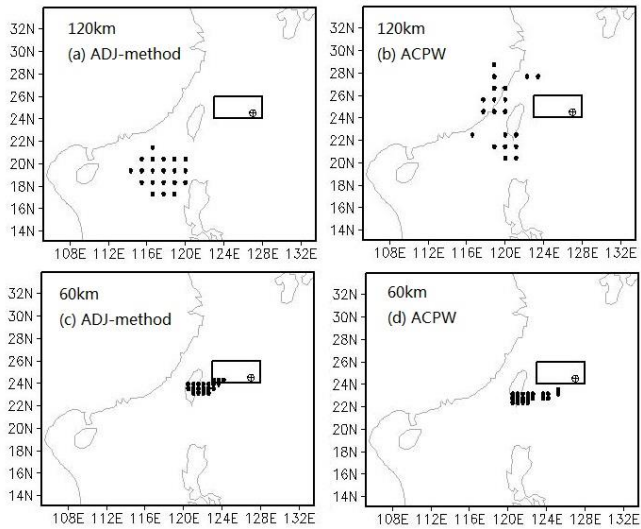


Figure 1011: Sensitive regions identified by the CNOPs with 20 points for TC Fitw. The squares indicate the verification areas, and the initial cyclone positions are shown as Θ . (a) and (b) denote the CNOP patterns at 120 km resolution for the ADJ-method and ACPW algorithm, respectively; (c) and (d) represent the CNOP patterns at 60 km resolution for the ADJ-method and ACPW algorithm, respectively.

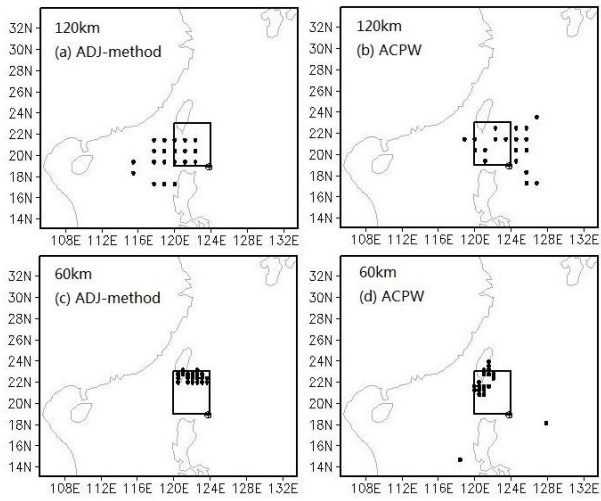


Figure H12: Sensitive regions identified by the CNOPs with 20 points for TC Matmo. The squares indicate the verification areas, and the initial cyclone positions are shown as Φ . (a) and (b) denote the CNOP patterns at 120 km resolution for the ADJ-method and ACPW algorithm, respectively; (c) and (d) represent the CNOP patterns at 60 km resolution for the ADJ-method and ACPW algorithm, respectively.

5

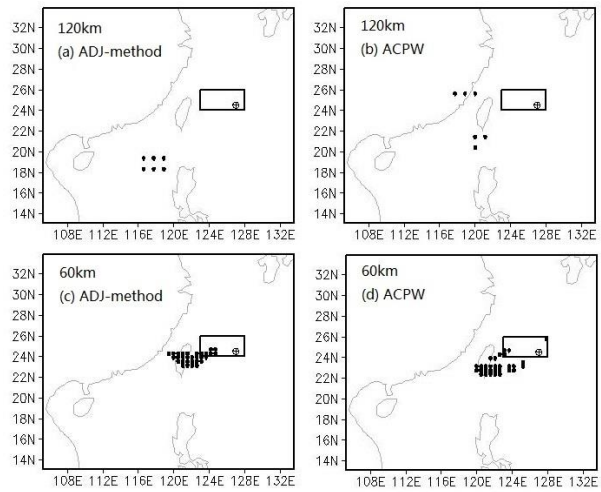
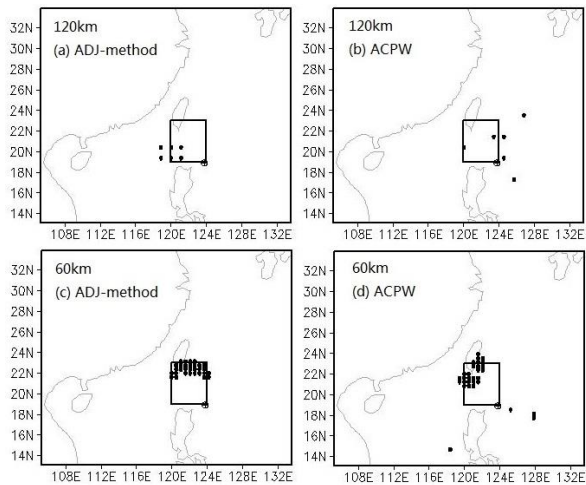


Figure 1313: Sensitive regions identified by the CNOPs with 6 points at 120 km resolution and 30 points at 60 km resolution for TC Fitow. The squares indicate the verification areas, and the initial cyclone positions are shown as Φ . (a) and (b) denote the CNOP patterns at 120 km resolution for the ADJ-method and ACPW algorithm, respectively; (c) and (d) represent the CNOP patterns at 60 km resolution for the ADJ-method and ACPW algorithm, respectively.



5

Figure 1314: Sensitive regions identified by the CNOPs with 6 points at 120 km resolution and 30 points at 60 km resolution for TC Fitow. The squares indicate the verification areas, and the initial cyclone positions are shown as Φ . (a) and (b) denote the CNOP patterns at 120 km resolution for the ADJ-method and ACPW algorithm, respectively; (c) and (d) represent the CNOP patterns at 60 km resolution for the ADJ-method and ACPW algorithm, respectively.

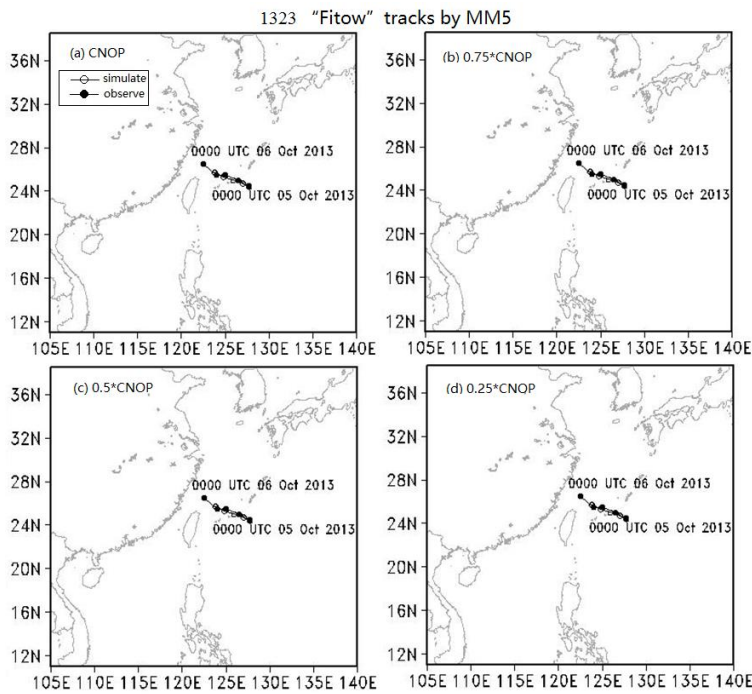


Figure 1415: Simulated TC tracks from MM5 by inserting the CNOPs or $W \times \text{CNOP}$ into the initial state in the entire domain for TC Fitow. Solid circles represent the observed TC tracks from the CMA, and the hollow circles show the simulated TC tracks from the MM5 model. (a), (b), (c) and (d) denote the CNOP, $0.75 \times \text{CNOP}$, $0.5 \times \text{CNOP}$ and $0.25 \times \text{CNOP}$ results, respectively.

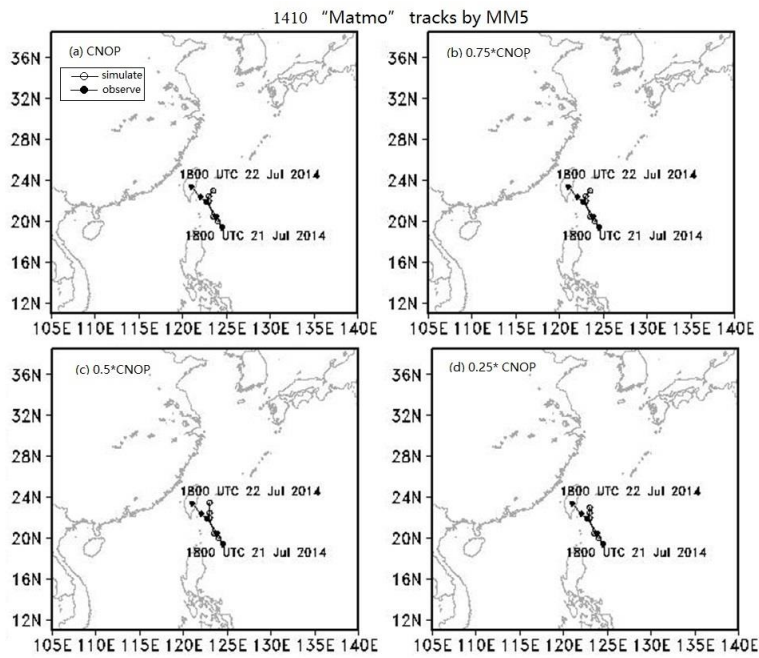


Figure 4516: Simulated TC tracks from MM5 by inserting the CNOPs or $W \times \text{CNOP}$ into the initial state in the entire domain for TC Matmo.

1323 "Fitow" tracks by MM5

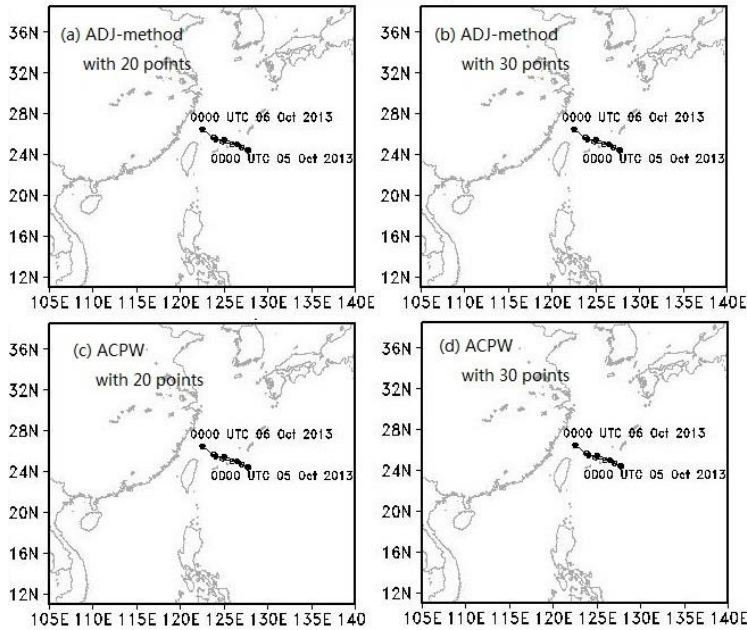


Figure 1617: Simulated TC tracks from MM5 by inserting the amended CNOPs, which are reduced by a factor of 0.5, in only the sensitive regions into the initial state for TC Fitow. Solid circles represent the observed TC tracks from the CMA, and the hollow circles show the simulated TC tracks from the MM5 model. (a), (b), (c) and (d) denote the ADJ-method with 20 points, ADJ-method with 30 points, ACPW algorithm with 20 points and ACPW algorithm with 30 points, respectively.

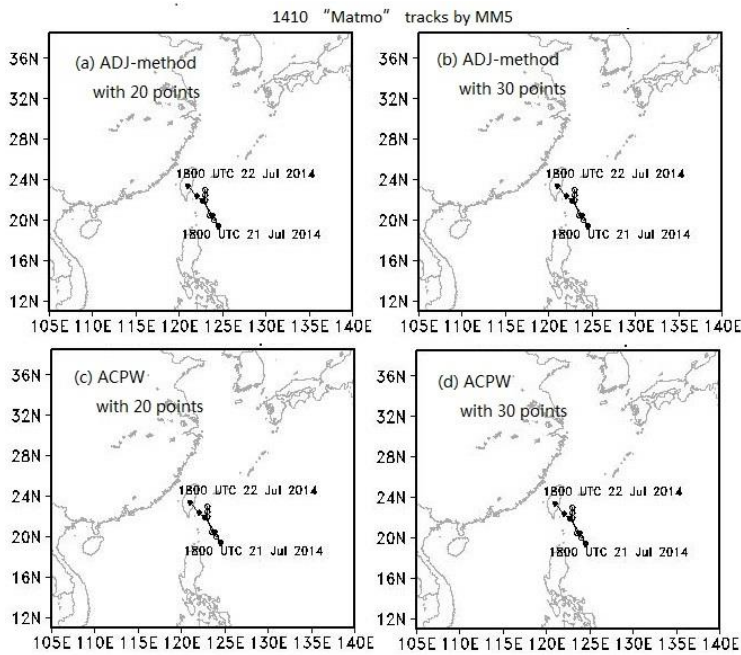


Figure 1718: Simulated TC tracks from MM5 by inserting the amended CNOPs, which are reduced by a factor of 0.5, in only the sensitive regions into the initial state for TC Matmo.

Table 1:

Name	Meaning	Value
n	Number of principle components	50
N	Number of individuals	420 at 120 km 200 at 60 km
a	Adaptive coefficient	Initial: 0.5
ω	Inertia coefficient	0.8
c1	Self-awareness to track the historically optimal position	2.05
c2	Social-awareness of the particle swarm to track the globally optimal position	2.05
Υ	Restraint factor to control the speed	0.729

θ	Velocity of individual	0.5
r	Local optimizing radius	$8 \times \delta / \text{original}$ dimensions
s	Step size of updating individual	0.6
p_a	Probability of individual escaping from current position	0.3
Total_Step	The number of iterations	50

Table 2: The meanings of all symbols.

Symbols	Values/components	Meanings
δu_0	$u'_0, v'_0, T'_0, p'_{s0},$	Initial perturbation
u_{NT}	$u'_t, v'_t, T'_t, p'_{st}$	Nonlinear evolution of perturbed U_0 at time t
D	Values rely on cases	Verification area
σ	(0, 1]	Vertical coordinate
c_p	1005.7 J kg ⁻¹ K ⁻¹	Specific heat at constant pressure
R_a	287.04 J kg ⁻¹ K ⁻¹	Gas constant of dry air
T_r	270 K	Constant parameter
p_r	1000 hPa	Constant parameter

Table 3: The analysis results of the PSO, WSA and ACPW methods.

Algorithm	Maximum Value	Minimum Value	Mean Value	RMSE
PSO	1034.192573	724.086002	900.7488578	0.121400896
WSA	1628.841294	323.7493169	930.9103862	0.431193448
ACPW	2240.275956	1243.377921	1542.505251	0.216750584

Table 4:

ACPW/ADJ-method	120 km	60 km
Fitow	-0.83	0.43
Matmo	0.42	0.37

Table 5: The ratios of energy for 24-h evolution by inserting the CNOPs from the ACPW algorithm and ADJ-method into the initial states.

ACPW/ADJ-method	120 km	60 km
-----------------	--------	-------

Fitow	94.1%	85.1%
Matmo	87.3%	70.2%

Table 6: Benefits (percent, %) gained from reducing the CNOPs by a factor of 0.5 in the sensitive regions identified by the ADJ-method and ACPW algorithm with 20 points.

Cases	Methods	60 km	120 km
Fitow	ADJ-method	3%	5.93%
	ACPW	-0.84%	8.05%
Matmo	ADJ-method	6.12%	20.90%
	ACPW	20.48%	16.26%

Table 7: Benefits (percent, %) gained from reducing the CNOPs by a factor of 0.5 in the sensitive regions identified by the ADJ-method and ACPW algorithm with 6 points at 120 km resolution and 30 points at 60 km resolution.

Cases	Methods	60 km (30 points)	120 km (6 points)
Fitow	ADJ-method	3.9	1.72%
	ACPW	4.23%	0.01%
Matmo	ADJ-method	1.21%	13.24%
	ACPW	9.75%	6.86%

5 **Table8: The time consumption of the ADJ-method and ACPW algorithm (unit: minutes).**

Methods	60 km	120 km
ADJ-method (1) ¹	79.9	12.4
ADJ-method (4) ¹	321.1	49.7
ACPW	20.8	2.74